Journal of Magnetism and Magnetic Materials 505 (2020) 166761

Contents lists available at ScienceDirect

Journal of Magnetism and Magnetic Materials

journal homepage: www.elsevier.com/locate/jmmm

Research articles

Estimation of dipole magnetic moment orientation based on magnetic signature waveform analysis by a magnetic sensor

Jiazeng Wang[a,b,c], Ying Shen[a,b,c,*], Rui Zhao[d], Chunkai Zhou[d], Junqi Gao[a,b,c,*]

[a] Acoustic Science and Technology Laboratory, Harbin Engineering University, Harbin 150001, China,
[b] Key Laboratory of Marine Information Acquisition and Security (Harbin Engineering University), Ministry of Industry and Information Technology, Harbin 150001, China
[c] College of Underwater Acoustic Engineering, Harbin Engineering University, Harbin 150001, China
[d] China Ship Development and Design Center, Wuhan 430064, China

ARTICLE INFO

Keywords:
Magnetic moment
Estimation
Magnetic anomaly signature

ABSTRACT

In this paper, we propose a measurement procedure to estimate the magnetic moment orientation (MMO) of a dipole. Theoretical analysis indicates that magnetic field in each orthogonal direction B_i (i = x, y, z) is found to be a superposition of its three basic elements B_{ij} (i = x, y, z and j = 1, 2, 3) along certain direction, allowing the obtained dipole signature to be decomposed of 9 basic elements. An orthogonal energy ratio (OER) algorithm is used to infer the MMO by calculating the signal energy distribution along each axis. A standard OER database is developed which provides a reference to be compared with the measured OER. The one having the smallest variance is determined as the estimated MMO. Owing to space symmetric property, it generally introduces 8 possible solutions. Then, a mathematic method is presented to define the common characteristics of the magnetic signature in the 8 octants, which is able to identify the octant of unknown target based on detected B_i field. As a result, the unique MMO can be estimated. The experimental results show good estimation accuracy for the dipole orientation with average error of 3.5°. In particular, the algorithm is independent of changing CPA and velocity, which is demonstrated in simulation and experiment.

1. Introduction

The fact that magnetic field transmission is indifferent to most medium of air, water, sea water, soils and human body allows magnetic sensors to be the eyes of many industrial and search systems. The application initiated in military reconnaissance, has spread into broad areas of mine prospect, traffic surveillance and intruder detection to sense the magnetic field anomaly. Within a search area, when the material moves over a stationary sensing system or when the sensors are mounted on a moving platform to sense a stationary material, the target manifest itself as unique voltage signal at the outputs of magnetic sensors. Though detection of an unknown magnetic target usually includes determination of both its position and magnetic moment, previous efforts have been extensively made to detect and localize the object by magnetic sensors [1,2], gradiometers [3], and networks [4]. For example, by extracting the obtained signal from background noise and applying the signal strengths into certain algorithms, the proximity to the target can be realized [1,2,5].

The magnetic moment is defined by orientation of that dipole and its magnetic strength. Estimation of the magnetic moment orientation (MMO) is always a concern in the community, which is an essential indicator to predict the hidden target behavior in many measurement settings. Unexploded ordnances (UXOs) contamination is a world-wide problem, and the success of any excavation is dependent on the accurate MMO determination of the underground dipole [6]. For intelligent traffic surveillance, the directions along which the ground or maritime vehicles are moving are determined by the dipole orientation [7–9]. Another search scenario is for the long, narrow sea cables and underground pipelines, which prefer to lie in the direction as the same as their MMOs [10,11]. More recently, in magnetic-controlled capsule endoscopy (MCE) application, it is necessary to take site-specific monitoring as detailed moment information is required for better diagnosis, drug delivery, biopsy and similar [12–14]. Indeed, without the ability of accurate estimation for MMO, these tasks can't be taken effectively. And recent studies have demonstrated that a 16 magnetic sensors array can achieve rather good MMO prediction with average error of 12° within a volume of 38 × 27 × 24 cm^3 [15]. However, employment of multiple sensors suffers from the bulky volume, high

* Corresponding authors at: Acoustic Science and Technology Laboratory, Harbin Engineering University, Harbin 150001, China.
E-mail addresses: shenying@hrbeu.edu.cn (Y. Shen), gaojunqi@hrbeu.edu.cn (J. Gao).

https://doi.org/10.1016/j.jmmm.2020.166761
Received 26 November 2019; Received in revised form 25 February 2020; Accepted 17 March 2020
Available online 19 March 2020
0304-8853/

cost, large computation load and system complexity. While the ability of using single magnetometer for MMO estimation, required for robust and compact sensing system, is still missing.

Our previous work indicates that the concealed target's behavior, like distance, velocity and moving direction, has a strong influence upon the magnetic signature waveform [16,17]. A typical dipole induced magnetic anomaly signatures are investigated with respect to two dependent parameters speed and CPA (closest path approach). The signature waveform width and sensing range angle are used to analyze the signatures. The signature waveform width T has been found to be proportional to the CPA but inversely proportional to the speed. It implies that the sensing range angle is independent of changing velocity and CPA. With a change in the motion direction, there is a reversal in its signature waveforms shape. These studies fuel a more profound inquiry, how to employ the magnetic fingerprint characteristics to obtain the dipole orientation information? Here, this letter reports the achievement for MMO estimation based on orthogonal energy ratio algorithm by a single magnetic sensor.

2. OER algorithm methodology

2.1. Theoretical background

According to the magnetic dipole detection theory, a ferromagnetic target can be considered as a magnetic dipole when the distance to sensors is at least three times larger than the largest dimension of the target. Firstly, a magnetic dipole model is established to analyze the magnetic anomaly signatures. Based on classic magnetic dipole model, the induced magnetic field $\vec{B}$ can be described as:

$$B(\vec{M},\vec{r}) = \frac{\mu_0}{4\pi}\left[\frac{3(\vec{M}\cdot\vec{r})\vec{r}}{|\vec{r}|^5} - \frac{\vec{M}}{|\vec{r}|^3}\right] \tag{1}$$

where $\mu_0 = 4\pi \times 10^{-7}$H/m is the space permeability, $\vec{r} = [x \;\; y \;\; z]^T$ is the position vector of the magnetic dipole, and $\vec{M} = [M_x \;\; M_y \;\; M_z]^T$ refers to the magnetic moment vector of the dipole. Equation (1) can be written into a matrix form as:

$$\begin{bmatrix} B_x \\ B_y \\ B_z \end{bmatrix} = \frac{\mu_0}{4\pi R^5}\begin{bmatrix} 3x^2 - R^2 & 3xy & 3xz \\ 3xy & 3y^2 - R^2 & 3yz \\ 3xz & 3yz & 3z^2 - R^2 \end{bmatrix}\begin{bmatrix} M_x \\ M_y \\ M_z \end{bmatrix} \tag{2}$$

where$R = |\vec{r}|$, and $[B_x \;\; B_y \;\; B_z]^T$ are the three components of $\vec{B}$ in each orthogonal direction. Fig. 1 shows a schematic dipole detection configuration comprised of a stationary magnetic sensor and a moving dipole. The sensor is assigned at the original point of the orthogonal coordinate system. In the x-y plane, the dipole is moving at a constant velocity v along x-axis, where the CPA (closest point approach) is set to be R_0. Thus, the position of the dipole relative to the sensor can be defined as:

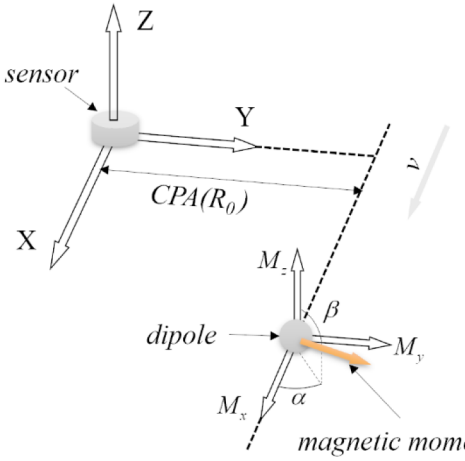

Fig. 1. Schematic diagram of a moving magnetic dipole and a stable magnetic sensor.

$$x = vt, \quad y = R_0, \quad z = 0 \tag{3}$$

In this model, the dipole orientation is defined by two angles α and β. α is used to describe the angle between the positive x-axis and projection of the dipole orientation into the x-y plane, and β is the angle between the magnetic moment and the positive z-axis. It can be observed that angle α ranges from 0 to 360° and angle β varies from 0 to 180°, respectively. Thus, the components of the magnetic moment can be written as:

$$M_x = sin\beta cos\alpha \; |\vec{M}|$$

$$M_y = sin\beta sin\alpha \; |\vec{M}|$$

$$M_z = cos\beta \; |\vec{M}| \tag{4}$$

Combining Eqs (3) and (4) into Eq. (2) results in:

$$\begin{bmatrix} B_x \\ B_y \\ B_z \end{bmatrix} = \frac{\mu_0 \; |\vec{M}|}{4\pi R_0^3}\begin{bmatrix} \frac{2(vt/R_0)^2 - 1}{(1+(vt/R_0)^2)^{5/2}} & \frac{3(vt/R_0)}{(1+(vt/R_0)^2)^{5/2}} & 0 \\ \frac{3(vt/R_0)}{(1+(vt/R_0)^2)^{5/2}} & \frac{3(vt/R_0)}{(1+(vt/R_0)^2)^{5/2}} & 0 \\ 0 & 0 & \frac{3(vt/R_0)}{(1+(vt/R_0)^2)^{5/2}} \end{bmatrix}\begin{bmatrix} \cos\alpha\sin\beta \\ \sin\alpha\sin\beta \\ \cos\beta \end{bmatrix} \tag{5}$$

We define a feature matrix $k(\gamma)$ as following:

$$k(\gamma) = \begin{bmatrix} \frac{2\gamma^2 - 1}{(1+\gamma^2)^{5/2}} & \frac{3\gamma}{(1+\gamma^2)^{5/2}} & 0 \\ \frac{3\gamma}{(1+\gamma^2)^{5/2}} & \frac{2-\gamma^2}{(1+\gamma^2)^{5/2}} & 0 \\ 0 & 0 & \frac{-\gamma^2 - 1}{(1+\gamma^2)^{5/2}} \end{bmatrix} = \begin{bmatrix} k_{x1}(\gamma) & k_{x2}(\gamma) & k_{x3}(\gamma) \\ k_{y1}(\gamma) & k_{y2}(\gamma) & k_{y3}(\gamma) \\ k_{z1}(\gamma) & k_{z2}(\gamma) & k_{z3}(\gamma) \end{bmatrix} \tag{6}$$

where $\gamma = vt/R_0$ is a dimensionless variable. Then equation (5) can take the following form:

$$\begin{bmatrix} B_x \\ B_y \\ B_z \end{bmatrix} = \frac{\mu_0 \; |\vec{M}|}{4\pi R_0^3}\begin{bmatrix} k_{x1}(\gamma) & k_{x2}(\gamma) & k_{x3}(\gamma) \\ k_{y1}(\gamma) & k_{y2}(\gamma) & k_{y3}(\gamma) \\ k_{z1}(\gamma) & k_{z2}(\gamma) & k_{z3}(\gamma) \end{bmatrix}\begin{bmatrix} \cos\alpha\sin\beta \\ \sin\alpha\sin\beta \\ \cos\beta \end{bmatrix} \tag{7}$$

To better understand equation (7), it can be decomposed into 9 basic elements as:

$$B_x = B_{x1} + B_{x2} + B_{x3}$$

$$B_y = B_{y1} + B_{y2} + B_{y3}$$

$$B_z = B_{z1} + B_{z2} + B_{z3} \tag{8}$$

Set $D = \mu_0 \; |\vec{M}|/(4\pi R_0^3)$ and each element could be represented as:

$$B_{x1} = Dcos\alpha sin\beta \cdot k_{x1}(\gamma)$$

$$B_{x2} = Dsin\alpha sin\beta \cdot k_{x2}(\gamma)$$

$$B_{x3} = Dcos\beta \cdot k_{x3}(\gamma)$$

$$B_{y1} = Dcos\alpha sin\beta \cdot k_{y1}(\gamma)$$

$$B_{y2} = Dsin\alpha sin\beta \cdot k_{y2}(\gamma)$$

$$B_{y3} = Dcos\beta \cdot k_{y3}(\gamma)$$

$$B_{z1} = Dcos\alpha sin\beta \cdot k_{z1}(\gamma)$$

$$B_{z2} = Dsin\alpha sin\beta \cdot k_{z2}(\gamma)$$

$$B_{z3} = Dcos\beta \cdot k_{z3}(\gamma) \tag{9}$$

An example is made to examine the waveforms characteristics of k_{ij}

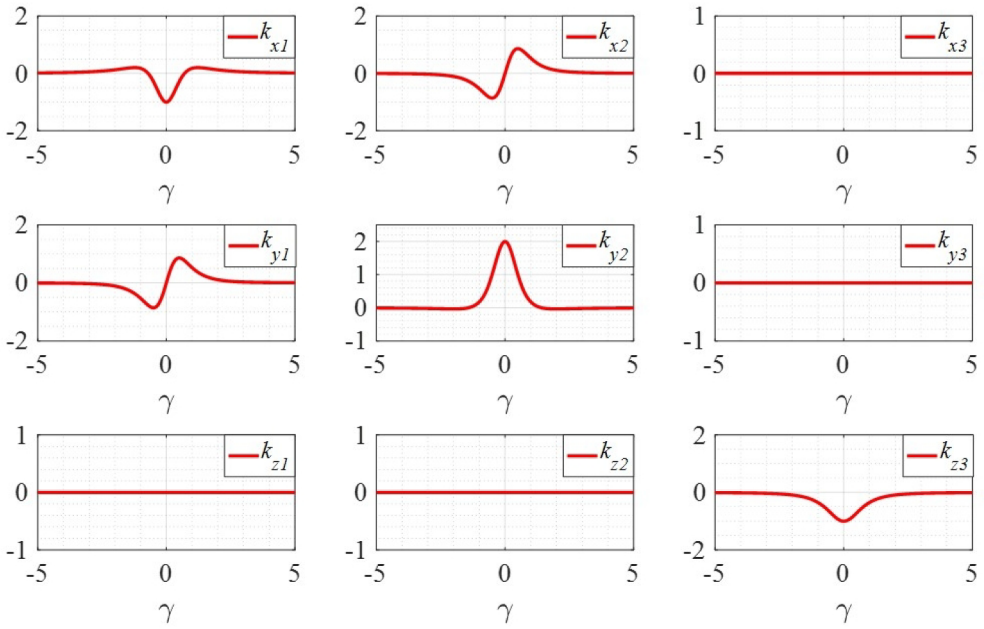

Fig. 2. Waveforms of 9 basic elements of k_{ij} at $\alpha = 137°$ and $\beta = 71°$. Nine k_{ij} elements are independent on α and β, producing characteristic waveforms with fixed shapes.

and B_{ij} (i = x, y, z and j = 1, 2, 3) given in Eqs (6) and (9). The waveforms of k_{ij} are shown in Fig. 2 on condition of $|\vec{M}| = 1A{\cdot}m^2$, $v = 1$ m/s, CPA = 1 m, $\alpha = 137°$, $\beta = 71°$. Equation (6) suggests that function k_{ij} is independent of α and β, producing characteristic waveforms with fixed shapes as illustrated in Fig. 2. In other words, the waveform patterns of the nine k_{ij} elements are always the same as shown in Fig. 2, which are immune of the changing angles of α and β.

In contrast, equation (9) implies that variables α and β assign different weights to each B_{ij} element in trigonometric terms, which should govern the waveform distributions of B_{ij} as shown in Fig. 3. As a result, a unique MMO defined by special combination of α and β would change the waveform patterns of B_{ij}, which vary from case to case and are not always as the way as this specific example shown in Fig. 3. Indeed, the inverse option to employ the induced B_{ij} signature characteristics open up the possibility to use such waveform configurations for target MMO identification.

2.2. OER algorithm

Firstly, the durations of measured magnetic signals must be determined for integration transformation need. Here, we define T as the valid signal width, which corresponds to 90% attenuation of the maximum total magnetic field of $B_T = \sqrt{B_x{}^2 + B_y{}^2 + B_z{}^2}$. Then the signal energy of each orthogonal axis within the duration T can be expressed as:

$$E_i = \int_T B_i^2(t)dt \quad (i = x, y, z)\# \tag{10}$$

Eq. (10) indicates that evaluation of E_i is highly dependent on T. To

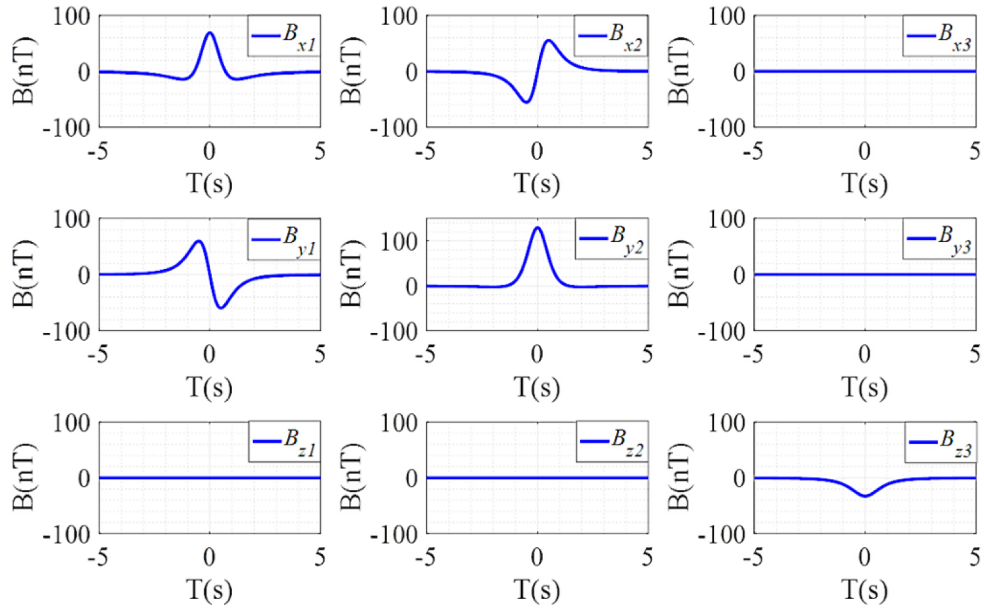

Fig. 3. Waveforms of 9 basic elements of B_{ij} at $\alpha = 137°$ and $\beta = 71°$.Waveform patterns of B_{ij} are dependent on α and β, which vary from case to case and are not always as this specific example shows.

obtain accurate T value, it is desirable to employ smoothing and high-pass filtering to preprocess the original signal in real measurement. Furthermore, in order to eliminate the effects from v, R_0 and $|\vec{M}|$, we normalize Eq. (10) to get their orthogonal energy ratio as following:

$$e_i = \frac{E_i}{E_x + E_y + E_z} \quad (i = x, y, z) \tag{11}$$

According to Eq. (11), a standard OER database is established by MATLAB on condition that v = 1 m/s, CPA = 1 m, $|\vec{M}|$ = 1A·m^2, α and β change from 0 to 360° and 0 to 180°, respectively. In this data library, OER under different combinations of α and β is a 360 × 180 × 3 matrix which is termed as [$S_x(\alpha, \beta)$, $S_y(\alpha, \beta)$, $S_z(\alpha, \beta)$]. Please note that the MMO evaluation is performed by scanning the database quickly to find the one having the smallest variance compared with the measured OER. Thus, the problem evolved into searching the sub-optimal orientation angles statistically among limited possible solutions. Then we can get an ambiguity plane $P(\alpha, \beta)$ as:

$$P(\alpha, \beta) = 10log\left(\frac{1}{\sum_i (S_i(\alpha,\beta) - e_i')^2}\right) i = x, y, z \tag{12}$$

where e_i'(i = x, y, z) are the three units of OER of the real signal. Obviously, the one has the largest P value is determined as the estimated MMO for the hidden target.

An example of the technique application is presented in Fig. 4 with MMO(α, β) = (137°, 71°). Applying data of B_x, B_y, B_z and T into Eqs (10)-(11) results in (e_x', e_y', e_z') = (0.287, 0.666, 0.047). In practical measurement, the data of B_x, B_y, B_z and T can be obtained by the outputs of a vector magnetic sensor. Then execution of variance scan in the OER database yields a typical ambiguity plane as shown in Fig. 4. It can be seen that there are 8 largest P values of 83.3 dB that emerge in the plane labeled by points *NO*. 1–8. Theoretically, P value must approach to be infinite, and the adopted computing accuracy limit around 10^{-8} accounts for P = 83.3 dB shown in this case. Because OER is a single channel of information on energy intensity, it produces 8 possible solutions in each octant due to spatial symmetry. The 8 possible MMOs are (47°, 71°), (137°, 71°), (227°, 71°), (317°, 71°), (47°, 161°), (137°, 161°), (227°, 161°) and (317°, 161°) in Octant 1–8, respectively.

Their corresponding magnetic signature waveforms are illustrated in Fig. 5. Though the OERs of these 8 MMOs are the same, they have different magnetic fingerprint curves in each octant as shown in Fig. 5. Such properties of magnetic signature waveforms are important for magnetic field detection, as illustrated by octant identification of dipole moment in the following section.

2.3. Octant determination

Based on Eqs (6) and (9), calculating integration of each element of matrix k in the range of -T/2 to T/2 using MATLAB, we can get:

$$\int_{-T/2}^{T/2} \frac{B_{x1}}{Dcos\alpha sin\beta} dt = \int_{-T/2}^{T/2} k_{x1}(vt/R_0)dt < 0 (cos\alpha sin\beta \neq 0) \tag{13}$$

$$\int_{-T/2}^{T/2} \frac{B_{y2}}{Dsin\alpha sin\beta} dt = \int_{-T/2}^{T/2} k_{y2}(vt/R_0 t)dt > 0 (sin\alpha sin\beta \neq 0) \tag{14}$$

$$\int_{-T/2}^{T/2} \frac{B_{z3}}{Dcos\beta} dt = \int_{-T/2}^{T/2} k_{z3}(vt/R_0)dt < 0 (cos\beta \neq 0) \tag{15}$$

$$\int_{-T/2}^{T/2} B_{x2} dt = \int_{-T/2}^{T/2} B_{y1} dt = 0 \tag{16}$$

Owing to Eqs (8)-(9), the magnetic field along each orthogonal direction can be found to be:

$$\int_{-T/2}^{T/2} B_x dt = \int_{-T/2}^{T/2} B_{x1} dt = Dcos\alpha sin\beta \int_{-T/2}^{T/2} k_{x1}(vt/R_0)dt \tag{17}$$

$$\int_{-T/2}^{T/2} B_y dt = \int_{-T/2}^{T/2} B_{y2} dt = Dsin\alpha sin\beta \int_{-T/2}^{T/2} k_{y2}(vt/R_0)dt \tag{18}$$

$$\int_{-T/2}^{T/2} B_z dt = \int_{-T/2}^{T/2} B_{z3} dt = Dcos\beta \int_{-T/2}^{T/2} k_{z3}(vt/R_0)dt \tag{19}$$

In order to simplify the relationship between the moment orientation and measured magnetic field $[B_x \quad B_y \quad B_z]^T$ shown in Eqs (17)-(19), a step function $h(\varepsilon)$ is given as:

$$h(\varepsilon) = \begin{cases} 1 & \varepsilon > 0 \\ 0 & \varepsilon \leq 0 \end{cases} \tag{20}$$

Applying equations (13)-(15) and (17)-(19) into (20), we can obtain the following equation as:

$$h_x = h\left(\int_{-T/2}^{T/2} B_x dt\right) = h(-cos\alpha sin\beta) \quad (cos\alpha sin\beta \neq 0)$$

$$h_y = h\left(\int_{-T/2}^{T/2} B_y dt\right) = h(sin\alpha sin\beta) \quad (sin\alpha sin\beta \neq 0)$$

$$h_z = h\left(\int_{-T/2}^{T/2} B_z dt\right) = h(-cos\beta) \quad (cos\beta \neq 0) \tag{21}$$

As angles α and β vary in the ranges of [0 360°] and [0 180°]

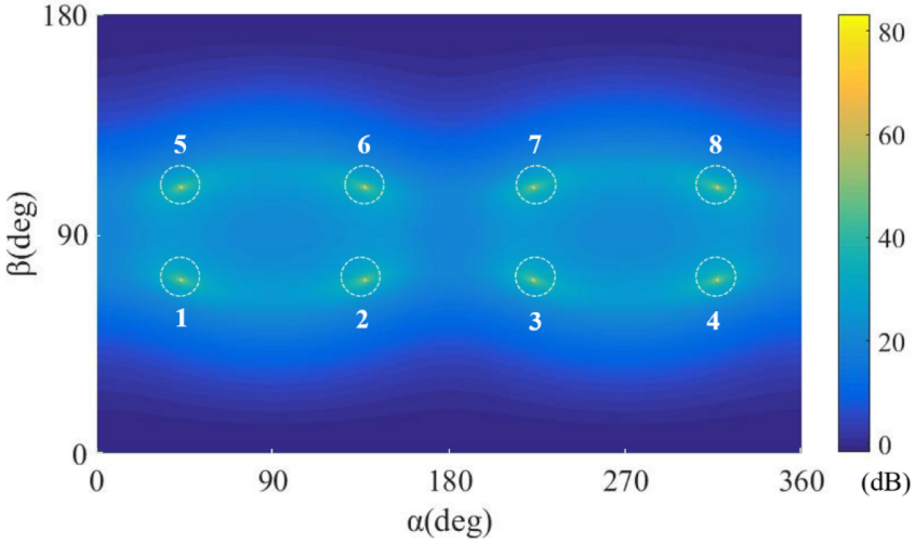

Fig. 4. A typical ambiguity plane with hidden target MMO(α, β) = (137°, 71°). Performance of proposed OER algorithm produces 8 possible solutions in each octant due to spatial symmetry.

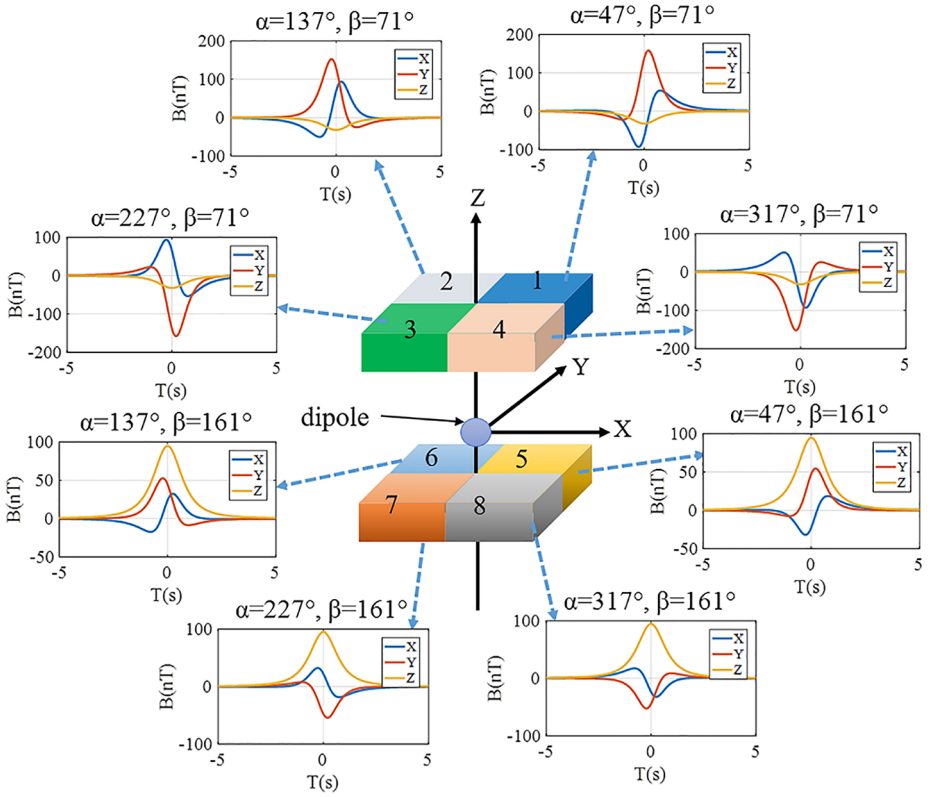

Fig. 5. Magnetic signature waveforms of 8 possible MMOs in each octant, which are (47°, 71°), (137°, 71°), (227°, 71°), (317°, 71°), (47°, 161°), (137°, 161°), (227°, 161°) and (317°, 161°).

Table 1
Matrices H for 8 octants.

α	(0°, 90°)	(90°, 180°)	(180°, 270°)	(270°, 360°)
β				
(0°, 90°)	H_1 = [0 1 0]	H_2 = [1 1 0]	H_3 = [1 0 0]	H_4 = [0 0 0]
(90°, 180°)	H_5 = [0 1 1]	H_6 = [1 1 1]	H_7 = [1 0 1]	H_8 = [0 0 1]

respectively. If the angles at the coordinate boundary are not considered, $H = [h_x\ h_y\ h_z]$ can be calculated by equation (21). The corresponding results of matrices H for 8 octants are summarized in Table 1. Indeed, the research interest is the reverse problem that by computing matrix H based on function (21), the MMO's octant can be determined owing to Table 1. Therefore, it provides an effective mathematic method to define the common characteristics of the magnetic signature in the 8 octants (see Fig. 5).

Continue to work on the example in section 2.2, and we can employ data of B_x, B_y, B_z and T into equation (21) to get H = [1 1 0]. It refers to octant H_2 where MMO(α, β) = (137°, 71°) (see Fig. 5). After execution of the whole OER algorithm, the estimated dipole moment can be determined, which corresponds well with the real one.

To summarize section 2, a schematic flow chart of proposed OER algorithm is illustrated in Fig. 6, which is comprised of three steps. Firstly, a theoretical model is introduced to obtain 9 basic elements of the magnetic field B_{ij}, whose magnetic signature waveforms are dependent of α and β(see Fig. 3). The second step is to develop a standard OER database [$S_x(\alpha, \beta)$, $S_y(\alpha, \beta)$, $S_z(\alpha, \beta)$] in a matrix of 360 × 180 × 3. It provides a standard library to compare with the measured OER, where the one having the largest P value (see equation (12)) is determined as the estimated MMO. Owing to space symmetric property, it generally introduces 8 possible solutions in each octant (see Figs. 4 and 5). In the last step, an octant determination procedure is applied to select the unique MMO by use of function (21) to group the uniform waveform features of the magnetic signature in the 8 octants. Through processing of the OER algorithm, the target MMO can be estimated. It should be noticed that if the target moves in an arbitrary route, the OER algorithm can work well to find the multiple possible solutions with space symmetry. However, to select the unique real octant, the proposed Octant Determination method shown in section 2.3 needs to be updated according to different routes.

3. Experimental demonstration

3.1. Experiment setup

The experimental setup comprises of a non-magnetic sliding track and a fluxgate magnetometer, as shown in Fig. 7. To mimic the theoretical detection model (see Fig. 1), the vector magnetometer is placed at the original point. And the sensor's three sensing directions are set as the coordinate system shows in Fig. 7 to enable measurement of the three magnetic field components B_x, B_y and B_z, respectively. A 1.5 mm thick magnet with 30 mm diameter is used as a magnetic dipole ($|\vec{M}| = 8.7\text{A}\cdot\text{m}^2$), which is placed on the bracket of the 1.8 m sliding track to move constantly at v = 0.3 m/s and CPA = 0.2 m in the test. The dipole orientation is fixed along its longitudinal direction perpendicular to its circular surface. The dipole orientation is changed by adjusting the attitude of the magnet.

3.2. Experiment results

There are four different dipole orientations set to be examined, which are MMO(α, β) = (45°, 45°), (135°, 45°), (225°, 135°) and (315°, 135°) in octant H_1, H_2, H_7 and H_8, respectively. As the four orientations are symmetric in space, the OER for them are equal to be (e_x, e_y, e_z) = (0.213, 0.501, 0.286) as shown in Table 2. The target induced magnetic

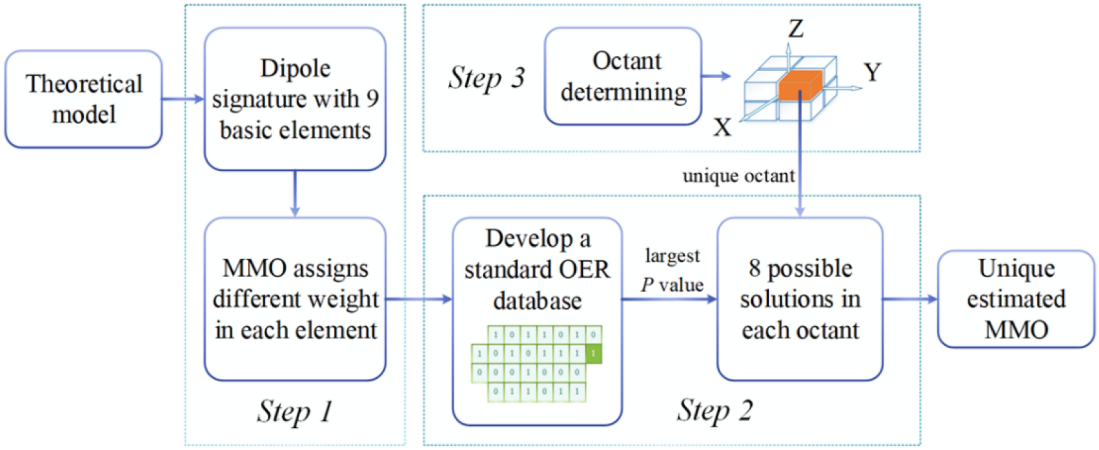

Fig. 6. Schematic flow chart of OER method.

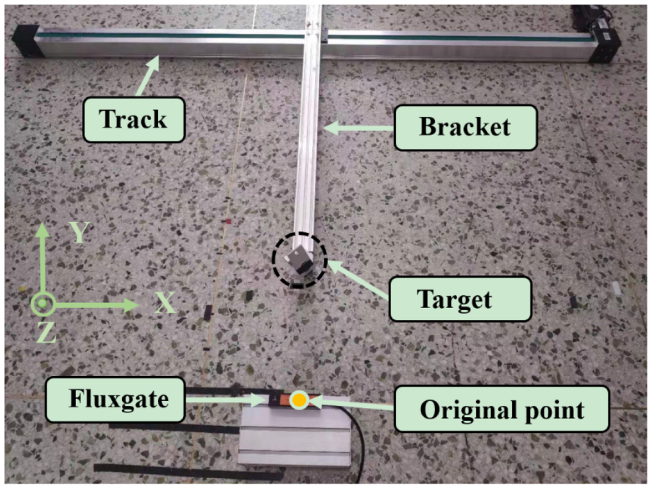

Fig. 7. Experiment setup picture including a non-magnetic slide track and a triple-axis magnetometer.

Table 2
Target MMO estimation results.

Real MMO (α, β)		(45°, 45°)	(135°, 45°)	(225°, 135°)	(315°, 135°)
Octant		H_1	H_2	H_7	H_8
Real OER	e_x	0.213	0.213	0.213	0.213
	e_y	0.501	0.501	0.501	0.501
	e_z	0.286	0.286	0.286	0.286
Estimated OER'	e_x	0.207	0.198	0.214	0.199
	e_y	0.506	0.485	0.478	0.439
	e_z	0.287	0.317	0.308	0.362
Estimated H		[0 1 0]	[1 1 0]	[1 0 1]	[0 0 1]
Estimated MMO (α, β)		(50°, 44°)	(131°, 42°)	(218°, 135°)	(324°, 138°)
Estimation error (α, β)		(5°, 1°)	(4°, 3°)	(3°, 0°)	(9°, 3°)

abnormal signal is sensed by the triple-axis fluxgate sensor. The obtained (B_x, B_y, B_z) is computed by the proposed OER algorithm, and the estimated MMO angles are shown in Table 2. Notice that measured OER are (e_x', e_y', e_z') = (0.207, 0.506, 0.287), (0.198, 0.485, 0.317), (0.214, 0.478, 0.308) and (0.199, 0.439, 0.362) respectively, which actually result in 8 solutions for each MMO. Performance of function (21) produces matrix H = [0 1 0], [1 1 0], [1 0 1] and [0 0 1], respectively. And the estimated MMO (α, β) = (50°, 44°), (131°, 42°) , (218°, 135°) and (324°, 138°) are obtained, which correspond to error(α, β) = (5°, 1°), (4°, 3°), (3°, 0°) and (9°, 3°), respectively. They correspond to average estimation error of 3.5°. This represents remarkable 3X of accuracy enhancement of dipole moment estimation over previous 16 magnetic sensors array method [15]. In particular, it is achieved by a single magnetic sensor. All data is summarized in Table 2. Besides, the estimation errors indicate that the evaluation accuracy varies in the four symmetric orientations. However, with respect to symmetrical MMOs, the proposed OER algorithm is an unbiased evaluation approach theoretically. Thus, the results suggest that the errors maybe largely arise from practical measurements.

It should be noted that good estimation can be achieved with respect to different dipole orientations in the case of real experiment. Though the experiment results have not been configured to allow for extremely precise determination of MMO, we believe that the errors are in an acceptable range, and supportive for the proposed evaluation method. These simulation and experiment data together demonstrate that OER method is an enabling technology for MMO determination.

4. Discussion

The OER algorithm is studied on assumption that the target velocity and CPA have no effect on estimation. To examine if it is true, then we investigate the effects of velocity and CPA by simulation and experiment.

4.1. Simulation

The effect of velocity is examined with v = 0.2, 0.3, 0.4, 0.5, 0.6, 0.7 m/s at constant CPA = 0.3 m; while the CPA is analyzed at CPA = 0.2, 0.25, 0.3, 0.35, 0.4 and 0.45 m with fixed v = 0.2 m/s when $|\vec{M}| = 1\text{A}\cdot\text{m}^2$, $\alpha = \beta = 45°$. The simulation results on velocity and CPA effects are shown in Fig. 8 (a) and (b), respectively. It can be directly seen that the estimated dipole moments are independent of changing v or CPA, and keep constant of (45°, 45°). The simulation results verify the assumption that the target velocity and CPA have no influence on the MMO estimation.

4.2. Experimental verification

An experiment is conducted accordingly to keep parameters α, β, v, CPA as the same as in the simulation in section 4.1. The MMO estimation results of magnetic moment direction under different velocity and CPA are shown in Fig. 9. It can be seen that the estimated MMOs have no obvious changes, and float slightly as a function of velocity and CPA, respectively. We believe the fluctuations in the estimated OER curves are mainly due to the measurement errors. As a result, we can see that the experimental results are basically consistent with the simulation data. These simulation and experiment results together demonstrate that the MMO estimation method based on OER algorithm is

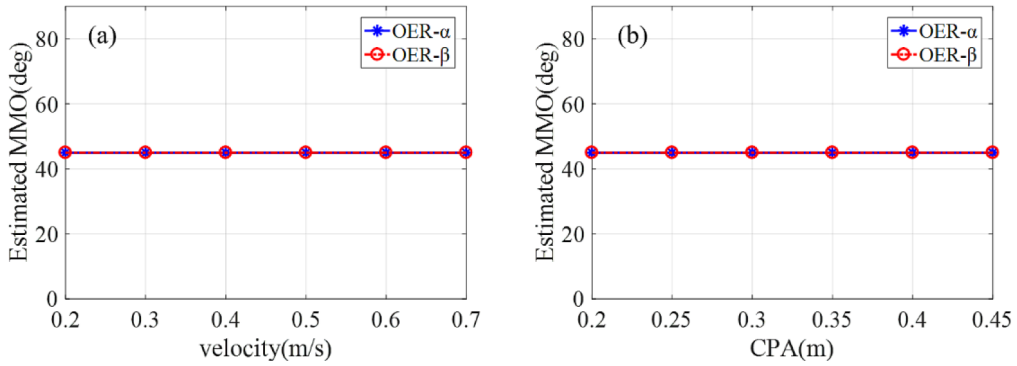

Fig. 8. (a) Effect of velocity on OER estimation; (b) Effect of CPA on OER estimation.

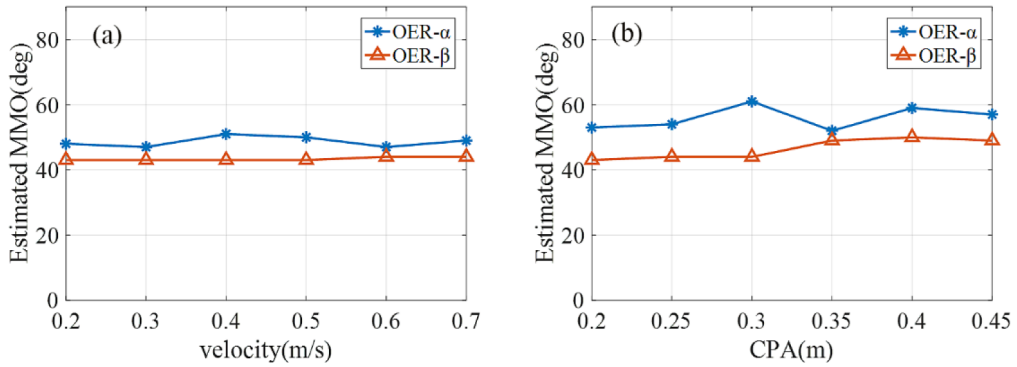

Fig. 9. (a) Effect of velocity on estimation; (b) Effect of CPA on estimation.

immune of changing velocity and CPA.

5. Conclusion

In summary, we have shown a dipole orientation evaluation method by a magnetic sensor using OER algorithm. Theoretical study indicates that moment direction gives different weights to each magnetic field element B_{ij}. Thus, the technology using the energy ratio develops a standard OER database that is able to find out optimum solution with the highest proximity to the measured target OER even if only one magnetometer is provided. Measurement results demonstrates good estimation with average error of 3.5°. This results in more than 3 times improvement in MMO estimation accuracy compared with previously reported array system. Moreover, the OER algorithm is independent of changing velocity and CPA, making it adaptable for wide applications. It should be seen that this work is focus on estimating the dipole MMO with known moving direction by single sensor. We are in progress to use two triple-axis sensors system to find the target random moving tracks.

The dipole orientation is proved to be manifest in the dipole energy signal. And the OER algorithm provides a reliable and straightforward mathematical approach to exploit such merit to determine the target MMO. The achievement of such one-sensor detection method promises compact, accurate, cost-efficient and low power dipole moment testing solution. When the dipole moves in a way arbitrarily, the octant determination analysis needs to be updated from case to case. In other words, this octant determination approach has its incapability to cover universal situations. To deal with this problem, we are trying to use an inversion method to estimate the real octant. Upon obtaining several possible solutions, the corresponding MAD signature for each of these possible solutions are modeled. After comparing with the real MAD signature fingerprints, the unique solution can be easily determined.

CRediT authorship contribution statement

Jiazeng Wang: Conceptualization, Methodology, Investigation, Formal analysis. **Ying Shen:** Funding acquisition, Supervision, Writing - original draft. **Rui Zhao:** Data curation, Software. **Chunkai Zhou:** Software, Validation. **Junqi Gao:** Funding acquisition, Supervision, Writing - review & editing.

Declaration of Competing Interest

The authors declare that they have no known competing financial interests or personal relationships that could have appeared to influence the work reported in this paper.

Acknowledgements

This work was supported in part by the Natural Science Foundation of Heilongjiang Province of China (LH2019E040) and the Academy of Space Electronic Information Technology (6142411183410). The project was supported by the China Ship Development and Design Center Grant (KY10500190043) and Acoustic Science and Technology Laboratory Grant (JCKYS2019604SSJS005).

References

[1] C.P. Du, M.Y. Xia, S.X. Huang, Z.H. Xu, X. Peng, H. Guo, Detection of a moving magnetic dipole target using multiple scalar magnetometers, IEEE Geosci. Remote Sens. Lett. 14 (2017) 1166–1170.
[2] Y. Shen, K.L. McLaughlin, J. Gao, D. Gray, L. Shen, Y. Wang, M. Li, D. Berry, J. Li, D. Viehland, AC magnetic dipole localization by a magnetoelectric sensor, Smart Mater. Struct. 21 (2012) 065007.
[3] Y.I.N. Gang, Z. Yingtang, L. Zhining, F. Hongbo, R. Guoquan, Detection of ferromagnetic target based on mobile magnetic gradient tensor system, J. Magn. Magn. Mater. 402 (2016) 1–7.
[4] J.T. Sherman, J.K. Lubkert, R.S. Popovic, M.R. DiSilvestro, Characterization of a Novel Magnetic Tracking System, IEEE Trans. Magn. 43 (2007) 2725–2727.
[5] B. Ginzburg, L. Frumkis, B.-Z. Kaplan, Processing of magnetic scalar gradiometer

signals using orthonormalized functions, Sens. Actuators, A 102 (2002) 67–75.
[6] S.D. Billings, C. Pasion, S. Walker, L. Beran, Magnetic models of unexploded ordnance, IEEE Trans. Geosci. Remote Sens. 44 (2006) 2115–2124.
[7] Y. Shen, J. Gao, D. Hasanyan, Y. Wang, M. Li, J. Li, D. Viehland, Investigation of vehicle induced magnetic anomaly by triple-axis magnetoelectric sensors, Smart Mater. Struct. 21 (2012) 115007.
[8] D. Liu, X. Xu, C. Fei, W. Zhu, X. Liu, G. Yu, G. Fang, Direction identification of a moving ferromagnetic object by magnetic anomaly, Sens. Actuators, A 229 (2015) 147–153.
[9] J. Zhou, J. Chen, Z. Shan, Spatial Signature Analysis of Submarine Magnetic Anomaly at Low Altitude, IEEE Trans. Magn. 53 (2017) 1–7.
[10] Z.Y. Guo, D.J. Liu, Q. Pan, Y.Y. Zhang, Forward modeling of total magnetic anomaly over a pseudo-2D underground ferromagnetic pipeline, J. Appl. Geophys. 113 (2015) 14–30.
[11] C. Yu, X. Xiang, L. Lapierre, Q. Zhang, Robust Magnetic Tracking of Subsea Cable by AUV in the Presence of Sensor Noise and Ocean Currents, IEEE J. Oceanic Eng. 43 (2018) 311–322.
[12] H. Zhou, G. Alici, A novel magnetic anchoring system for wireless capsule endoscopes operating within the gastrointestinal tract, IEEE/ASME Trans. Mechatron. 24 (2019) 1106–1116.
[13] S. Zhang, T. Sun, Y. Xie, C. Yu, S. Jin, J. Yu, H. Mao, Clinical efficiency and safety of magnetic-controlled capsule endoscopy for gastric diseases in aging patients: our preliminary experience, Dig. Dis. Sci. 64 (2019) 2911–2922.
[14] J.C. Norton, P.R. Slawinski, H.S. Lay, J.W. Martin, B.F. Cox, G. Cummins, M.P.Y. Desmulliez, R.E. Clutton, K.L. Obstein, S. Cochran, P. Valdastri, Intelligent magnetic manipulation for gastrointestinal ultrasound, Science Robotics, 4 (2019) eaav7725.
[15] G. Shao, Y. Tang, L. Tang, Q. Dai, Y. Guo, A novel passive magnetic localization wearable system for wireless capsule endoscopy, IEEE Sens. J. 19 (2019) 3462–3472.
[16] Y. Shen, D. Hasanyan, J. Gao, Y. Wang, J. Li, D. Viehland, A magnetic signature study using magnetoelectric laminate sensors, Smart Mater. Struct. 22 (2013) 095007.
[17] Y. Shen, J. Wang, J. Shi, S. Zhao, J. Gao, Interpretation of signature waveform characteristics for magnetic anomaly detection using tunneling magnetoresistive sensor, J. Magn. Magn. Mater. 484 (2019) 164–171.